SYMPOSIUM 1988
TRONDHEIM

CAVITATION EROSION OF HYDRAULIC MACHINES: GENERATION AND DYNAMICS OF EROSIVE CAVITIES.

François AVELLAN IMHEF-EPFL Switzerland
Philippe DUPONT IMHEF-EPFL Switzerland

SUMMARY

The cavitation which causes severe erosion of hydraulic machine runners is produced by the development of fixed cavities attached at the leading edge of the blades. It is clearly shown, from a comparison between the observations of cavity patterns during model tests and the damage found in the prototype, that the damaged areas of the blades extend in the wake of the fixed cavities. In this paper we give experimental evidence that this damage is due to the collapse of transient cavities in the fixed cavity closure region. Visualizations, pressure measurements and LDA flow field measurements using the IMHEF High-Speed Cavitation Tunnel allow us to describe the generation and the dynamics of these transient cavities where the Reynolds number plays a leading role. Moreover the investigation carried out with a special facility, the Cavitation Vortex Generator, reveals that the spherical shock-waves emitted in the last stages of cavity collapse are strong enough (20 kbar) to damage any industrial alloy. These experimental results should be confirmed in order to provide a physical basis for numerical simulation of the fixed cavity development and the generation-collapse cycle of the related transient cavities.

RESUME

L'érosion sévère des roues de machines hydrauliques est due à un type de cavitation particulier, représenté par le développement d'une cavité stationnaire attachée au bord d'attaque des aubes. Il résulte des comparaisons effectuées entre les figures de cavitation observées durant les essais en cavitation sur modèle et les dégâts rencontrés sur prototype que ceux-ci s'étendent dans une zone de l'aubage située dans le sillage de ces cavités attachées. Dans cette publication, nous apportons la preuve expérimentale que ces dégâts sont dus à l'implosion de cavités transitoires dans la région de fermeture de la cavité attachée. Des visualisations et des mesures de pression jointes à des sondages de vitesse par LDA dans le Tunnel de Cavitation à Grande Vitesse de l'IMHEF nous permettent de décrire la génération et la dynamique de ces cavités transitoires où le nombre de Reynolds joue un rôle prépondérant. D'autre part, les études menées sur une installation spéciale, le Générateur de Vortex Cavitants, ont montré que les ondes de choc sphériques qui sont émises dans les stades ultimes de l'implosion sont suffisamment fortes (20 kbar) pour endommager n'importe quel alliage industriel. Ces résultats expérimentaux doivent être confirmés afin de fournir une base physique aux simulations numériques à la fois du développement de ces cavités attachées et du cycle génération-implosion des cavités transitoires qui leur sont associées.

INTRODUCTION

In order to avoid erosion problems, hydraulic machine manufacturers should define a reliable setting level for both pumps and turbines. To achieve this, cavitation tests are carried out on models and in the first instance, a setting level is selected with an adequate safety margin, referred to a hydraulic performance criterion regardless of the type of cavitation involved in the actual tests. Since this criterion is based on the measured influence of the cavitation on any selected hydraulic parameter such as head, efficiency or power, unless this simple practice can be successfully used on small units, this type of criterion is not suitable for the accurate determination of the setting of large units. In this case, the method must be improved by carrying out cavitation observation during model tests [1]. Moreover, owing to the development of new computerized methods [2], which allow us to optimize the cavitation behavior of the hydraulic profiles, see [3], the problem of the cavitation erosion of the machine during the off-design operation at high loads rapidly arises, unless the actual setting level does not lead to any cavity development in the usual operating range.

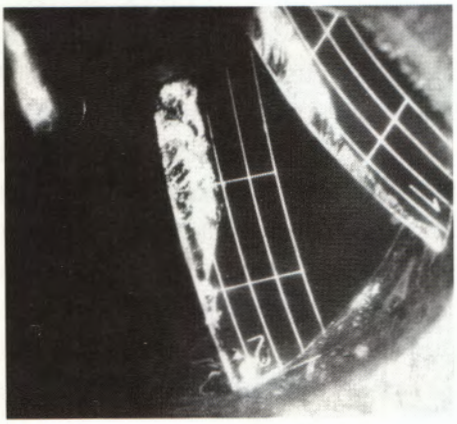

Figure 1: Leading edge cavitation on an $n_q = 45$ storage pump model; 10 mm between each white line on the blade suction side, $\dot{V}/\dot{V}_A = 0.9$; $\sigma = 0.147$

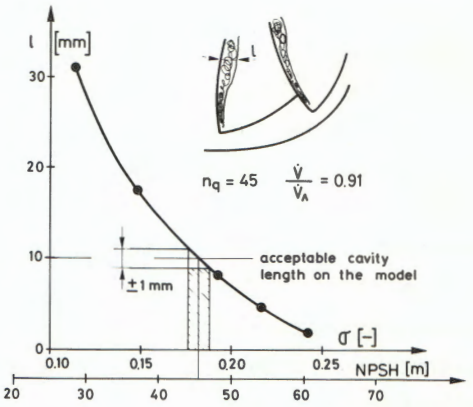

Figure 2: Influence of the cavitation number on the leading edge cavity length for the $n_q = 45$ storage pump model.

As Gülich and Pace have pointed out, in the case of centrifugal pumps, the leading edge cavity length is a macroscopic parameter strongly related to cavitation erosion [4]. Thus, an acceptable cavity length (Figure 1) can be defined empirically as a reference for the setting determination, but this length obviously depends on the nominal head of the actual machines. Furthermore, the resulting setting level is very sensitive to the cavity length when the cavity is visible on the suction side. For instance, a typical length evolution, with cavitation number σ, is given in Figure 2. The reported values were obtained during a cavitation test on an $n_q = 45$ storage pump model at the IMHEF laboratory. All the model design requirements for acceptance tests were fulfilled, in particular a rigorous geometrical homology with the prototype, and large windows installed at the inlet cone. Even under the best experimental test conditions, it was difficult to measure this length with an accuracy better than 1mm on the blade. By taking into account this uncertainty on the curve for the 10 mm which corresponded to the

acceptable cavity length values, the calculations gave a σ value of 0.182 within a range of $\pm$ 0.006. Since in this case the nominal head of the prototype was 250 m, the setting level could be estimated at 45.5 m to within $\pm$ 1.5 m. It should be emphasized that this uncertainty is due only to a lack of accurate observation, without taking account of the arbitrary character of the acceptable length definition. Moreover, for a high discharge operating point, in the case of centrifugal pumps, the cavity which extends on the blade pressure side is not visible.

To overcome these difficulties, and in order to answer a simple question such as which cavity length is acceptable, we have tried to study the basic mechanisms involved in the cavitation erosion of hydraulic machines. The approach followed is based on experimental tools corresponding to three levels of observation. The first stage involved identifying the type of cavitation associated with the severe erosion of hydraulic machines by comparing cavity patterns during model tests and the damage found in the corresponding prototype. This type of cavitation was then studied on a 2-D blade profile installed in the test section of the IMHEF High-Speed Cavitation Tunnel [5]. Both the stationary and the transient flow fields are investigated in the case of a fixed cavity using visualizations, wall pressure measurements and Laser Doppler Anemometry (LDA). The influence of the Reynolds number on the mean characteristics of the fixed cavity and on the dynamics of the U-shaped transient cavities convected downstream is studied. Finally, we carry out microscopic observation of the transient cavity life cycle, growth and collapse, by using an original facility, the Cavitation Vortex Generator. This facility, whose mode of hydraulic operation and related equipment are described elsewhere [6], was found [7] to be able to erode specimens in the same way as the erosion observed in both hydraulic machines and blade profiles in our High-Speed Cavitation Tunnel. A high-speed camera allows us to record the cavitation vortex collapse in this facility.

IDENTIFICATION OF THE EROSIVE CAVITIES

As we consider severe cavitation erosion in a hydraulic turbomachine, excepted for the particular case of Pelton turbines, we decide to restrict our field of investigation to the operating point of industrial interest. That means we only consider the damage to the runner which occurs during "normal" operation of the unit. This excludes the off-design range of operation such as a partial load where one can observe development of swirling motion in the blade-to-blade volume. In order to identify the type of cavitation associated with erosion, it is necessary to compare the cavity pattern during cavitation tests corresponding to the plant setting with the damaged area found in the prototype during periodic field visits. Due to the time lag between acceptance tests and start-up of the industrial machine and the variability of hydro-power generation, only a few cases are available for making these comparisons. Nevertheless, we can examine among them two cases for which the data were sufficiently reliable to provide identification of the erosive cavities.

The first case concerns an $n_q = 32$ storage pump, of which the impeller was found to be damaged after 1,250 hours of operation, under a nominal head of 440 m. Though the impeller was made of cast stainless steel, severe erosion took place on the suction sides of the blades, see photograph in Figure 3-a. Since, for a centrifugal pump, the operating range extends only along one head-discharge characteristic, the comparison with observations of the cavity pattern on a model is made simpler than in

the case of a turbine. According to the inlet flow vector diagram, this damage is due to the onset of leading edge cavitation on the suction side, resulting from a high incidence flow at a lower discharge than the nominal one. The second photograph (Figure 3-b), taken during the cavitation tests, shows the development of a fixed leading edge cavity at the same setting level as the prototype ($\sigma=\sigma_{plant}$).The correspondence between the two photographs is clearly visible. The damaged area definitely extends downstream of the fixed stationary cavity. This suggested to us that transient cavities are convected in the wake of the fixed cavity and then collapse on the blade surface. Evidence of these transient cavities can be found by careful examination of the second photograph, in which U-shaped vaporous vortices can be observed downstream of the fixed cavity closure.

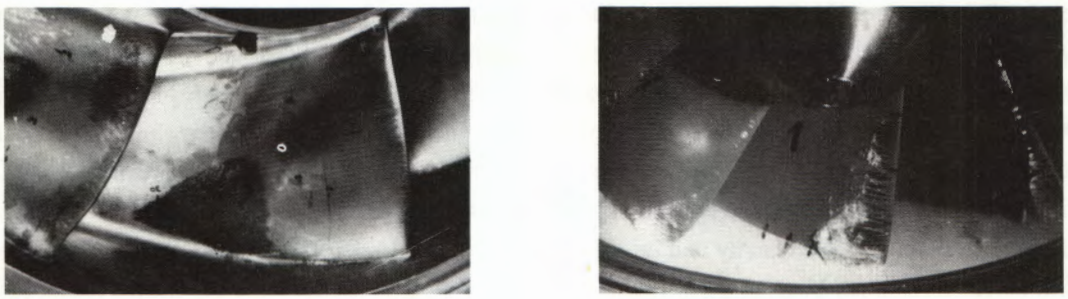

3-a **3-b**

Figure 3: Relation between blade erosion and leading edge cavitation in an $n_q = 32$ storage pump. **3-a** Photograph of the damaged area on the blade suction side of the prototype impeller; nominal head Hn = 440 m; 1,250 hours of operation. **3-b** Leading edge cavitation on the model impeller at the plant cavitation number: $\dot{V}/\dot{V}_{\wedge} = 0.87$.

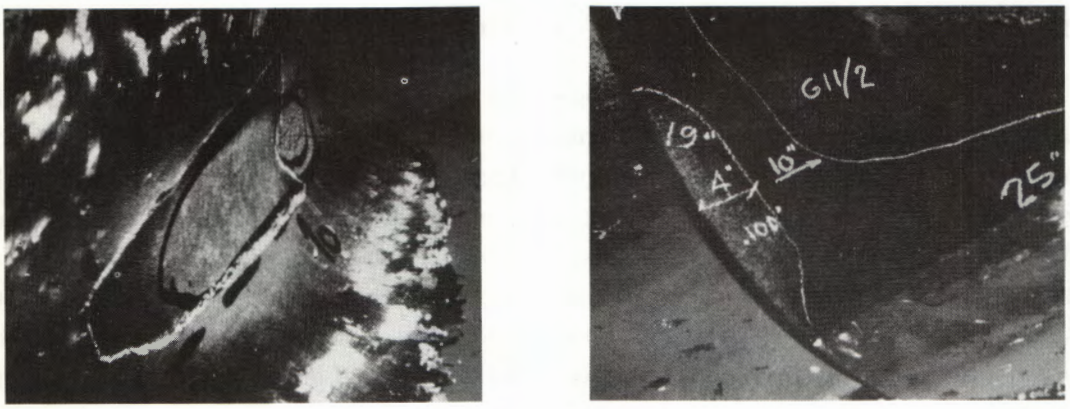

4-a **4-b**

Figure 4 Photographs of the prototype runner of an $n_q = 66$ Francis turbine after 17,000 hours of operation; nominal head Hn = 80 m; nominal power 190 MW. **4-a** View of the suction side of the runner inlet edge. **4-b** View of the suction side of the blade trailing edge at the runner outlet.

The second case presented concerns a Francis turbine with a specific speed of $n_q = 66$ ($\nu = 0.42$). The prototype with a nominal power of 190 MW operates under a nominal head of 80 m . A first inspection, after 5,000 hours of operation, led to a repair, by welding with Stellite 21, the area limited by the white contour in the photograph of the prototype runner inlet edge shown in Figure 4-a.

This part of the runner was made in 308 stainless steel as a preventive measure. The two photographs in Figure 4 were taken during a second inspection after 17,000 hours of operation, 12,000 hours after the previous field repair. The coating of paint was removed from every blade in the area of the fillet between the inlet edge of the suction side and the shroud (see Figure 4-a). Pitting was observed on the region limited by the black contour; maximum erosion took place at 18 % of the chord, just upstream of the Stellite layer which was only roughened. Pitting was also observed at the outlet on the suction side of the blades, Figure 4-b.

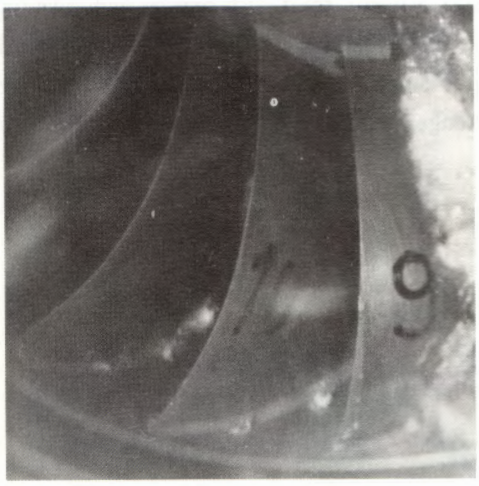

Figure 5-a Cavitation test at the plant cavitation number, the operating point corresponds to the full load and the nominal head ; $\dot{V}/\dot{V}_{\Lambda} = 1.13$.

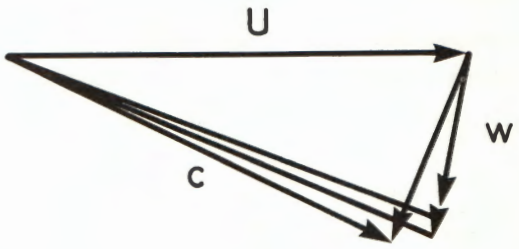

Figure 5-b Theoretical inlet flow vector diagrams at the inlet edge-shroud junction; 90% of the full load, $\dot{V}/\dot{V}_{\Lambda} = 0.99$; 95% of the full load, $\dot{V}/\dot{V}_{\Lambda} = 1.04$ and full load, $\dot{V}/\dot{V}_{\Lambda} = 1.13$.

If, in turn, we consider the cavitation tests on the model at the contractual loads, 90%, 95% and 100% respectively, for the nominal head coefficient which is 2% higher than that of the best operating point, the observations reveal an inlet cavitation development in the region which corresponds closely to the region of the damage. This inlet cavitation has the same pattern in the three cases; a full three-dimensional cavity attached to the blade leading edge followed by transient cavities for which the swirling motion is well marked as it is shown in the photograph of Figure 5, taken for the plant cavitation number and corresponding to the full load operation. According to the theoretical inlet flow vector diagrams of Figure 5, corresponding to the previous three operating points, the formation of the cavity is due to high incidence flow, as in the case of the centrifugal pump. The strong swirling motion of the transient cavities seems to be produced by the shearing of the flow in this part of the runner as will be seen in the next section. However, it appears certain that the damaged areas on the blades extend in the wake of the fixed cavity. In the region of the cavity closure, unsteady vortex cavity structures are created and advected downstream by the mean flow to the pressure recovery region of the flow field. In these regions, the repeated vortex cavity collapses lead to damage of the material of the blade wall, resulting in severe erosion of the blade surface.

LEADING EDGE CAVITATION FLOW

Despite considerable advantages of doing cavitation tests on model machines, the relatively low test head, no more than 40 m in practice, and difficult access to the flow prevent us from studying leading edge cavitation related to erosion in the machine test-rig facility itself. Thus, we decided to investigate this type of cavitation on a two-dimensional blade profile installed in the test section of the IMHEF High-Speed Cavitation Tunnel. This Tunnel (see Figure 6) is specially designed for the study of cavitation in a velocity range of technical interest. A velocity of 50 m/s can be reached in the rectangular test section of 150 mm x 150 mm x 750 mm. The test section is equipped with optical windows for good visualization and to improve the LDA signal-to-noise ratio. The blade studied has a symmetrical NACA 009 profile with a maximum thickness of 10 mm, it is truncated at 90% of the chord and the resulting chord length is 100 mm. A revolving bed plate flange provides a rigid mounting base for the blade with the possibility of varying the incidence angle.

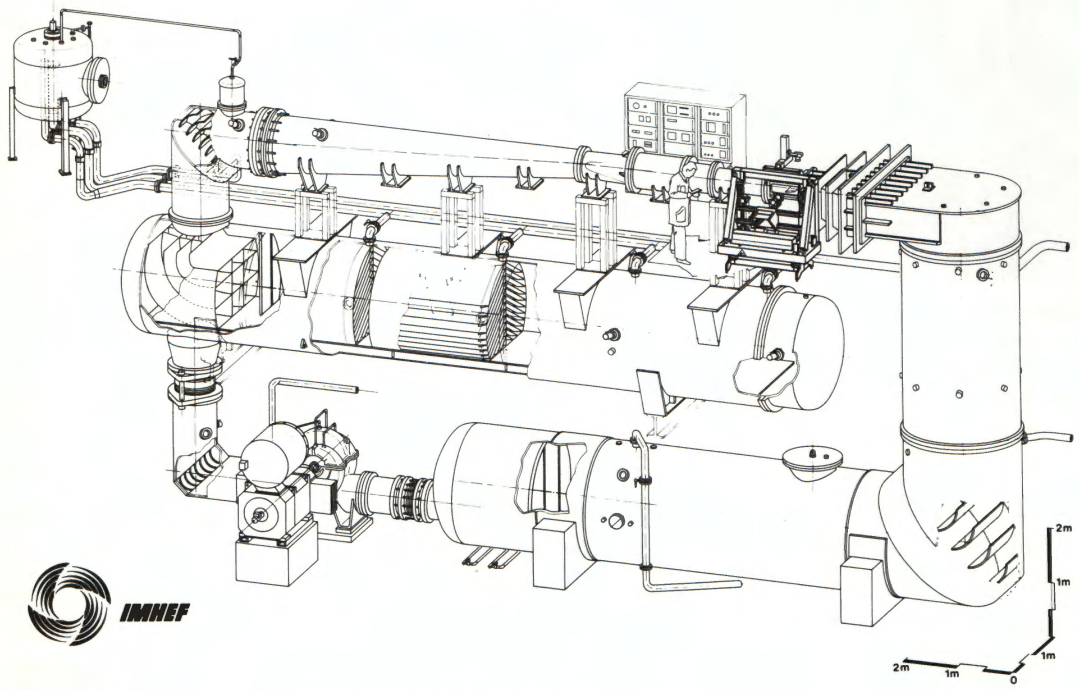

Figure 6 View of the IMHEF High-Speed Cavitation Tunnel ;
Rectangular test section: 50 m/s maximum velocity, absolute pressure from vapor tension to 7 bar; tunnel static pressure: up to 16 bar; double-suction pump: head of 35 m, flow rate 1.125 m^3/s at 700 RPM; minimum transit time 98 s, Minimum bubble collected 100 μm diameter.

Since our aim is to study the basic physical process by which leading edge cavitation can be erosive, we decided to restrict our experiments to a given flow geometry. That means we study the cavitation flow corresponding to a given hydrodynamic blade profile, a given flow incidence and a given cavitation number. These conditions are related to the model testing of a hydraulic machine as if we were carrying out a cavitation test with a given runner, for the same combination of a wicket gate opening, and a pressure coefficient at a given cavitation number. For the following operating conditions: 2.5° incidence angle and a 0.81 cavitation number referred to the inlet of the test section, we observe the development of

a stationary cavity attached to the blade leading edge (see photograph in Figure 7). The detachment of the stationary cavity occurs from a regular spanwise distribution of spots which develop downstream as cavity cones with a shiny appearance of the interface. From the first 10% of the chord length, all these cones are brought together to form the cavity itself. The mixing process between the rolling-up of the sides of each cone leads to the triggering of a laminar to turbulent transition, revealed by the foamy aspect of the cavity interface. Due to the strong instabilities of the last part of the cavity, it is not easy to define accurately where it ends, but the mean location of the cavity closure could be roughly estimated to 30% of the chord length for an upstream velocity of 20 m/s. In the closure region, transient cavities are produced, organized with an inverse U-shaped swirling structure, which is the same as the one previously observed in the photographs of the cavitation model tests.

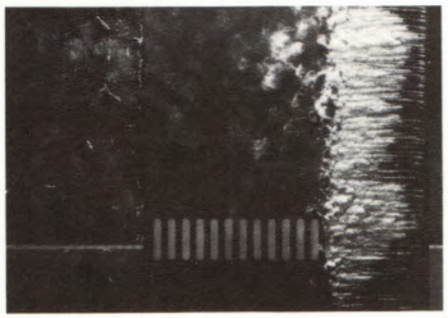

Figure 7: Upper view of a fixed leading edge cavity in the IMHEF Cavitation Tunnel test section (flow from left to right), NACA 009 blade profile, chord length L = 100 mm, incidence angle i = 2.5°, cavitation number $\sigma = 0.81$, upstream velocity, $U_\infty = 20$ m/s

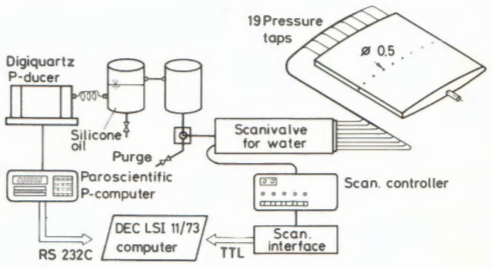

Figure 8 Diagram of the IMHEF pressure acquisition system

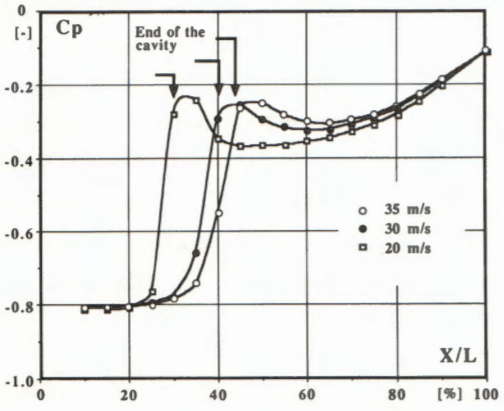

Figure 9 Influence of the Reynolds number on the experimental wall pressure distribution on the suction side of the NACA 009 blade, the apparent cavity length is reported for each velocity, i =2.5°,$\sigma = 0.81$

Visualizations made for the same operating parameters, but for different upstream velocities, show the strong influence the Reynolds number of the flow has in the mean length of the fixed cavity. As long as the upstream velocity increases, the cavity length varies from 30% of the chord length at 20 m/s to 45% at 35 m/s. This result is confirmed by the wall pressure measurements carried out on the blade suction side for 3 different upstream velocities, 20 m/s, 30 m/s and 35 m/s. These measurements are provided by a water pressure line scanning system connected to the streamwise-distributed blade 0.5 mm diameter pressure taps (see Figure 8). The different pressure distributions are given in Figure 9 by plotting against the pressure tap location on the blade chord, the pressure coefficient

Cp referred, as usual, to the upstream static pressure p_v and to the upstream dynamic pressure $\frac{1}{2}\rho U_\infty^2$. With this choice of pressure references, the vapor pressure level p_v corresponds to the negative value of the cavitation number (0.81), as it is the case in Figure 9, on the dry part of the blade. The pressure recovery of up to a -0.25 Cp value is the same in the three cases, and it occurs upstream of the apparent cavity closure location obtained by visualizations. Moreover, as it increases, the Reynolds number leads to a reduction in the pressure recovery gradient, as the velocity deceleration decreases. The strong influence of the Reynolds number suggests to us that the dynamics of the swirling structures plays a leading role on the mean pressure distribution.

If we write the normalized form of the Bernoulli equation of the mean flow by considering a stream line passing through the point O, in the vicinity of the main cavity, and a downstream point M, located in the cavity closure region, we obtain :

$$\mathbf{Cp}(M) + \sigma = \frac{U_O^2 - U_M^2}{U_\infty^2} + \frac{1}{\mathbf{Fr}^2}\frac{2(Z_O - Z_M)}{L} - \zeta$$

$$\text{with } Cp = \frac{p - p_\infty}{\frac{1}{2}\rho U_\infty^2}; \quad \sigma = \frac{p_\infty - p_v}{\frac{1}{2}\rho U_\infty^2} \quad \text{and} \quad Fr = \frac{U_\infty}{\sqrt{gL}}$$

where ρ is the water density, g is the gravity acceleration and L the blade chord length.

The Froude number **Fr** of the flow appears in relation to the setting levels Z_O and Z_M of points O and M. The ζ number represents the head loss coefficient corresponding to the velocity fluctuations integrated from O to M. Only this coefficient, which in the particular case of the boundary layer is the friction coefficient, can be increased by the Reynolds number of the flow, or more exactly by the Reynolds number of the large swirling structures. Therefore, if we consider the above Bernoulli equation for two points located on the cavity, we have $Cp = -\sigma$; an increase in ζ produces a decrease in the dynamic pressure term U_M^2/U_∞^2 over the cavity. Since this term will be less influenced downstream of the cavity closure, we should have a decrease of the acceleration of the fluid. This is confirmed by a decrease in the pressure recovery gradient observed in Figure 9 at 35 m/s. The increase of the cavity length with the Reynolds number also means that the energy transfer from the mean flow to the large structures is detrimental to the mean pressure.

The two dimensional LDA measurements of the mean velocity components, Vx,Vy and of the mean Reynolds stress tensor components $\overline{V'_x{}^2}$, $\overline{V'_y{}^2}$ et $\overline{V'_x V'_y}$ give us an insight into the behavior of these large structures. On the Vx profiles in Figure 10-a, a velocity defect is apparent downstream of the main cavity closure. The Vy profiles in Figure 10-b indicate a strong deviation of the flow after the first station at 10% of the chord. This deviation propagates downstream to reach a vertical extension of 10 mm at the cavity closure which does not exceed 2 mm in height and then this deviation is diffused up to the blade trailing edge. The strong variation in the profiles in Figure 10 suggests to us that vortices are created from the first 10% of the blade; they are convected to the outer part of the flow with an inflexion of their trajectory at 45% of the chord. Integration of the stream lines obtained from the set of this experimental data by solving the differential equation : $dy/dx = V_y/V_x$ shows clearly, in Figure 11, the

mean trajectory of these vortices, with their rapid vertical extension over the cavity and a reduction of their convective velocity.

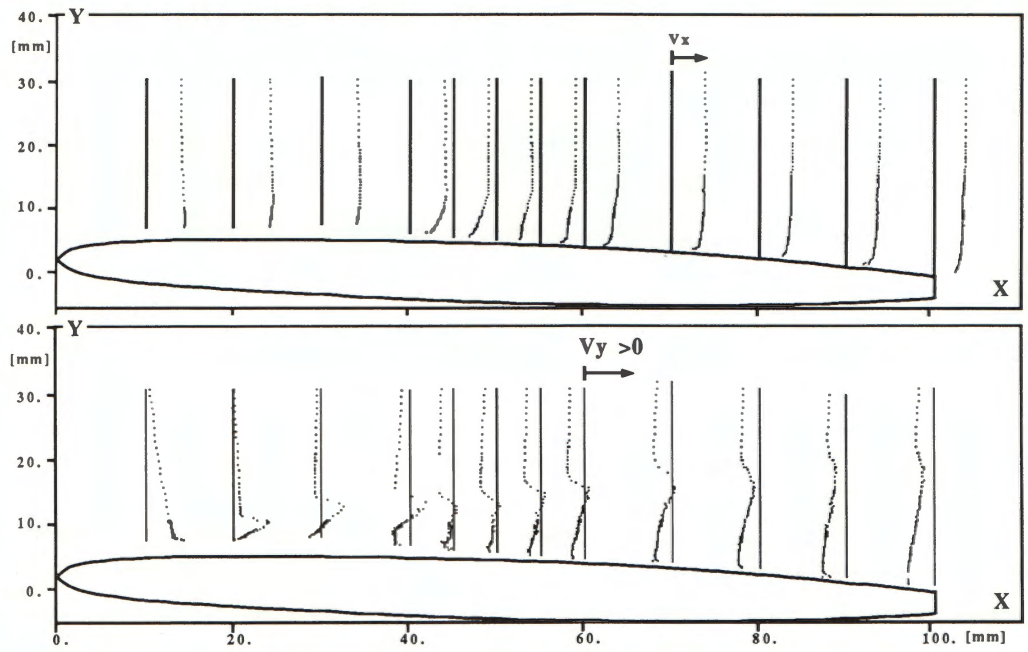

Figure 10 LDA measurements of the mean flow field over the NACA 009 blade suction side; i = 2.5°, σ =0.81, U_∞ = 20 m/s. **(a)** Profiles of the longitudinal component Vx of the mean velocity, **(b)** Profiles of the transverse component Vy of the mean velocity

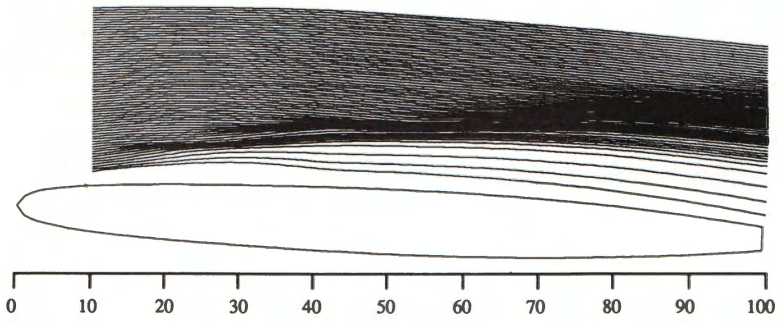

Figure 11
Mean stream lines integrated from the experimental LDA data over the NACA 009 blade suction side; i = 2.5°, σ =0.81, U_∞ = 20 m/s.

According to the expression of the head loss coefficient obtained by projecting the equation of the mean momentum conservation on a mean stream line and by neglecting the viscous effect, we have after integration:

$$\zeta = \frac{1}{\frac{1}{2}\rho U_\infty^2} \int_O^M \left[\vec{\nabla} . \bar{\bar{\tau}}_t \right] . \vec{t}\, ds \quad \text{with} \quad \bar{\bar{\tau}}_t = -\rho\, \overline{\vec{v}' \otimes \vec{v}'} \quad \text{the Reynolds stress tensor}$$

and $\vec{t}$ the tangent vector of the stream line of curvilinear abscissa s.

Since the experimental data for the Reynolds stress tensor components are available, we can simply integrate the Bernoulli equation along the stream lines already obtained in Figure 11 , in order to determine the pressure field in the bulk flow.

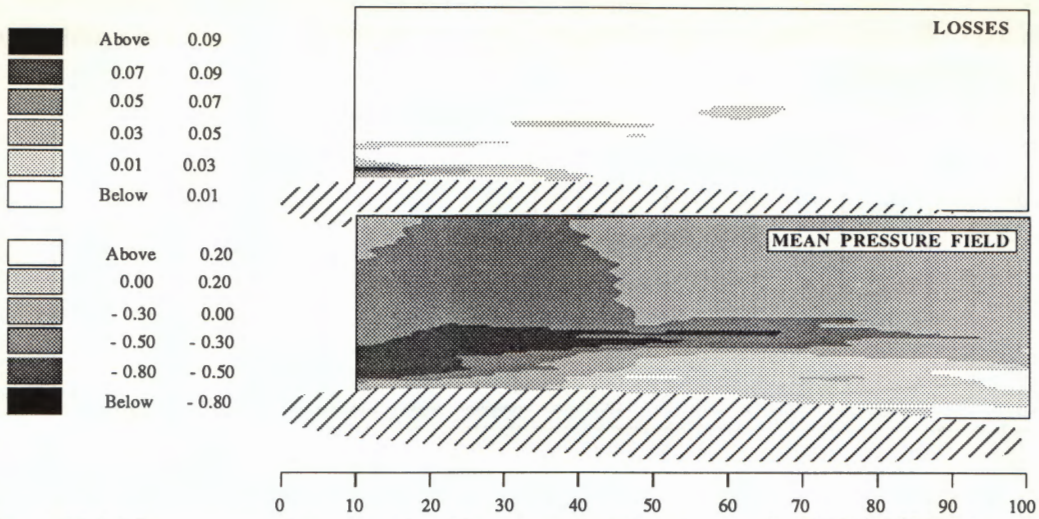

Figure 12 (a) Iso-contour of the mean head losses per length unit over the NACA 009 blade suction side; $i = 2.5°$, $\sigma = 0.81$, $U_\infty = 20$ m/s, and **(b)** iso-contour of the mean static pressure field.

The results of the integration are reported in Figure 12-b in the form of an iso-pressure contour map, and Figure 12-a the contours of iso-head losses per unit length ζ are also reported. The strong energy transfer to the travelling vortices, which takes place in the region of the cavity closure, should be pointed out. It agrees with the hypothesis of the leading role played by these cavities in the influence of the Reynolds number on the increase of the cavity length. In order to illustrate this influence, we reported in Figure 13 the pressure distribution along the stream line, closest to the blade wall that we could reached. The two curves in Figure 13 are obtained by integration of the experimental data with and without taking into account of these head losses. These curves show the same trend as the pressure distribution curves in Figure 9; a decrease of the pressure recovery gradient and of the static pressure as the losses are increased.

DYNAMICS OF THE TRANSIENT CAVITATION VORTICES

Both visualizations and LDA experiments show that the transient cavities which occur in the flow region of the leading edge cavity closure originate from discrete flow structures shed from the beginning of the cavity. The shedding of the discrete structures comes from the instabilities of the mean spanwise vorticity lines which are strongly perturbed by the streamwise rolling-up of the multiple cavity cones which takes place at the leading edge. The stretching of the discrete structure vorticity lines by the mean flow field (Kelvin-Helmholtz instabilities) leads to the rapid vertical extension of their mean trajectory as can be seen from the mean stream lines in Figure 11. A strong energy transfer from the mean static pressure field to the kinetic energy of these swirling structures takes place in the cavity closure region where there is maximum loss (see Figure 13). In this region, which corresponds to the wake of the leading edge cavity, the vorticity of the swirling structures is increased by a quantity proportional to U_{ext} / δ_s where δ_s is the sheared layer thickness at this station and U_{ext} the corresponding external velocity. The vorticity increase leads to the production of the U-shaped transient cavities by a vaporization of the swirling structure cores or a vapor dragging from the main cavity to the center of these discrete vortices (see Figure 14).

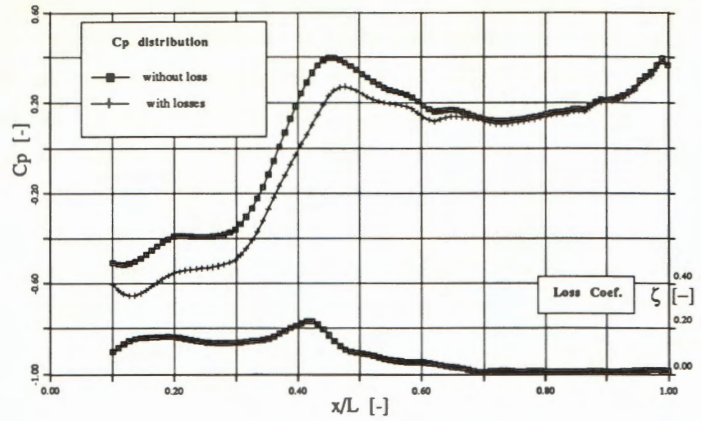

Figure 13 Influence of the losses in the pressure distributions, integrated with and without taking into account the losses along the stream line closest to the blade wall; $i = 2.5°$, $U_\infty = 20$ m/s $\sigma = 0.81$.

The cavitation vortices are then advected downstream and sweep the blade wall with their tips according to the Helmholtz theorem. In the high pressure region, the vortex cavity collapses occur close to the blade wall, producing severe damage to the material. Since the formation mechanism of these cavities is driven by the energy transfer in the sheared flow region of the leading edge cavity, a Strouhal number St could be built from the structure shedding frequency **f**, the thickness δ_s and the external velocity U_{ext}. From the experimental values taken at 40% of the chord length where the maximum shear stress is reached ($\delta_s = 10$ mm, $U_{ext} = 1.2\ U_\infty$, $U_\infty = 20$ m/s), we obtain a value of 0.46 of the Strouhal number corresponding to a shedding frequency **f** = 1.110 kHz, obtained by visualizations. Moreover, we find, also from visualizations at 30 m/s and 35 m/s respectively, a corresponding shedding frequency value of 1.875 kHz and 2.330 kHz. By assuming that the Strouhal number remains constant, the linear increase of the shedding frequency of the cavitation vortices with the upstream velocity implies that the vorticity of the cavitation vortices will follow the same linear increase with the upstream velocity according to the following expression: $\frac{U_{ext}}{\delta_s} = St\,.\,\mathbf{f}$

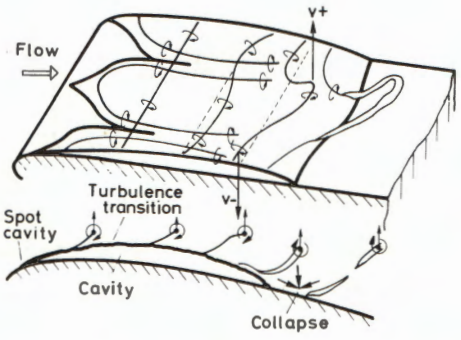

Figure 14 Sketch of the discrete structure shedding over a fixed leading edge cavity and the subsequent U-shaped cavitation vortices formation in the closure region.

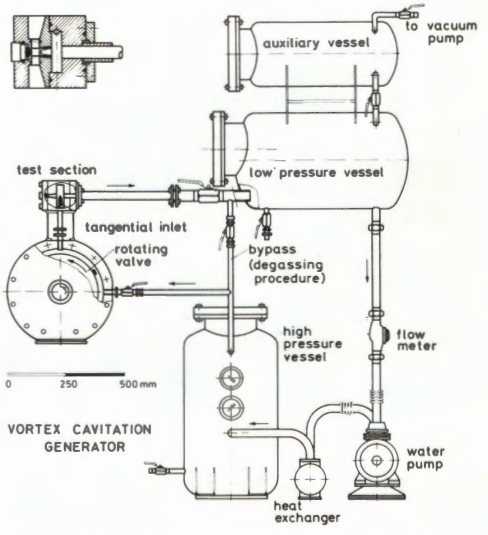

Figure 15 Diagram of the IMHEF Cavitation Vortex Generator

In order to have an insight into the dynamics of a single cavitation vortex, we used the Cavitation Vortex Generator (CVG) where cavitation vortices can be isolated and studied in the test section. The tangential inlet flow, (see Figure 15) induces a rotational motion in both the test section and the outlet pipe, which are aligned along the same axis. According to the Helmholtz vortex law, the vorticity line extends downstream to the vessel and upstream to an axisymmetric stagnation point at the end of the truncated volume. In the center part of the flow, the viscosity effect leads to a free vortex flow field with a solid body rotation core. At the cut-off of the flow by the rotating valve, the resulting water-hammer generates an expansion wave which promotes vaporization within the core of the vortex flow. When the valve opens, the resulting overpressure forces the cavitation vortex to collapse. A sequence of a cavity collapse obtained with a Cranz-Schardin high-speed camera is shown in Figure 16. The very short frame period of 3 μs allows us to record the cavity wall motion and the propagation of the shock-waves. We can observe the break-up of the cavity core into several individual cavities which collapse successively. In spite of the irregularities of the cavities, the shock-waves have spherical symmetry; moreover, these waves seem to be weak enough not to alter the motion of the main cavity which is attached to the wall. In Figure 17, the radius of each visible wave is added to the height of their respective radiative center and plotted against the frame number. The length of the main cavity is also reported. Except for the time of the collapse of a neighboring cavity, the cavity length decreases with a constant acceleration of - 0.95 m/s^2. The collapse, resulting in spherical shock-waves, and the rebound of the cavity can be seen very well after the 13th frame. By assuming an identical motion between the collapse and the cavity rebound, we can estimate the wall motion velocity at 640 m/s and the shock-wave celerity at 3,050 m/s, which corresponds to a Mach number of 2.06. The calculation from these data of the overpressure through the shock front gives an overpressure within a range of 19.5 - 25.4 Kbar (1,950 - 2,540 MPa), which corresponds to the fact that cavitation can cause the plastic deformation and subsequent erosion of any industrial alloy, even Stellite. One example of the crater caused by a cavitation vortex collapse on a 9060 Stellite placed in the CVG is shown in Figure 18.

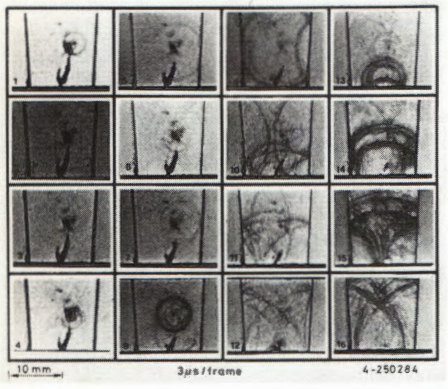

Figure 16 Final stage of the cavitation vortex collapse followed by spherical shock-waves; frame period 3μs, exposure time 300 ns, nominal flow rate 3.0 m^3/h, valve velocity 203 RPM.

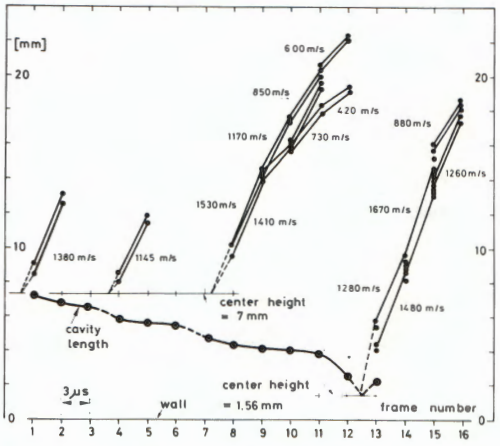

Figure 17 Time evolution of the main cavity length of the previous sequence and the corresponding shock-waves radii. The reflected wave speeds are underlined.

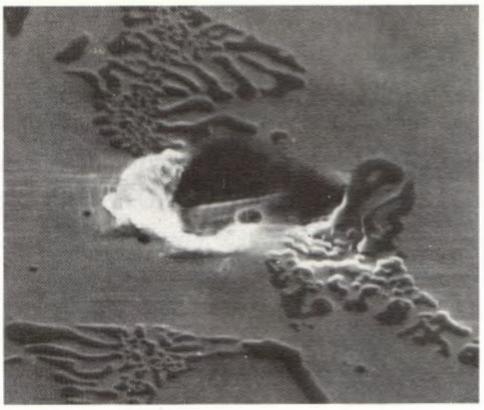

Figure 18 Photograph taken by scanning electron microscopy of a crater produced on a Stellite specimen in the Cavitation Vortex Generator. Crater diameter approx. 5 μm.

CONCLUSIONS

We have studied the cavitation which causes the most severe damage to hydraulic machine runners. By performing systematic comparisons, as far as possible, between the observations of cavity patterns during model tests and the damage found in the prototype, we are able to determine that the damaged area of the blades extends in the wake of a fixed leading edge cavity. Erosion of the blade material is due to the collapse of U-shaped transient cavities, which are advected with a swirling motion downstream of the leading edge cavity closure. By using the IMHEF High-Speed Cavitation Tunnel, we studied the development of a turbulent leading edge cavity over a two-dimensional blade for upstream velocities close to the one reached in the field of hydraulic machine. The role of the large discrete structures generated in the cavity detachment zone is revealed by systematic LDA flow field measurements. The existence of these structures leads to a strong effect on the static pressure losses, since an increase in the Reynolds number results in an increase in the mean cavity length. In addition, the shedding of these discrete structures at the blade leading edge is driven by the energy supply in the closure region of the main cavity, in such a way that the vorticity of these discrete swirling structures is increased as the Reynolds number is increased. Furthermore, the energy transfer from the mean flow to these large structures induces the production of the U-shaped transient cavities in the cavity closure region, which are advected downstream where the collapse takes place. The frequency shedding of these U-shaped transient cavities is found to be proportional to the upstream velocity. Moreover, the high-speed visualization of the cavitation vortex collapse in a special facility allows us to record the fast motion of the cavity. The most important phenomenon is the formation of spherical shock-waves, produced by the cavity rebound, after the final stage of the collapse shock-wave overpressure of more than 2,000 MPa was measured, which gives us an idea of the aggressiveness of this type of transient cavity. We have already be able to provide a precise description of the basic hydrodynamic processes by which fixed leading edge cavitation could erode the blade material. However, in order to establish a quantitative prediction model of the production rate and the intensity collapse of the cavitation vortices for this particular type of cavitation, we plan to perform spectral analysis of the transient flow field for different upstream velocities, and to determine whether the Strouhal number of the shedding cavities remains effectively constant. We also intend to take systematic measurements of the shock-wave overpressure as related to the vorticity of the cavitation vortex.

ACKNOWLEDGEMENT

The authors wish to acknowledge the contribution made by all their colleagues from the IMHEF Cavitation Research Group. They especially thank Mr. Vullioud from the Vevey Engineering Works and Dr. Simoneau from IREQ who kindly provided the photographs of the prototype runners. This work is supported financially by the Swiss Federal "Commission d'Encouragement à la Recherche Scientifique", The Swiss energy producers association "Nationaler Energie Forschung Fonds", The Sulzer Brothers company and the Vevey Engineering Works company.

REFERENCES

[1] Canavelis, R. , Lapray, J.F. and Rey, R. ,1986, "Etude d'un critère de fiabilité vis-à-vis de l'érosion par cavitation dans les pompes", *Proceedings of 13th I.A.R.H. Symposium on Progress in Technology*, 2-5 September, 1986, Montréal, vol.I, pp 43-1, 43-15.

[2] Favre, J.N. , Avellan, F. and Ryhming, I.L. , 1987, "Cavitation Performance Improvement by using a 2-D Inverse Method of Hydraulic Runner Design", *Proceedings of Int. Conf. on Inverse Design Concepts and Optimization in Engineering Sciences-II (ICIDES)*, 26-28 October, 1987, Pennsylvania State University (USA), pp.15-1, 15-15

[3] Favre, J.N. and Walther, W. , 1986, "Analyse de la cavitation d'entrée d'un aubage Kaplan par l'application d'une méthode de calcul inverse bi-dimensionnelle", *Proceedings of 13th I.A.R.H. Symposium on Progress in Technology*, 2-5 September, 1986, Montréal, vol.1, pp 4-1, 4-14 .

[4] Gülich, J.F. , Pace, S.E. , 1986, "Quantitative Prediction of Cavitation Erosion in Centrifugal Pumps", *Proceedings of 13th I.A.R.H. Symposium on Progress in Technology*, 2-5 September, 1986, Montréal, vol.I, pp 42-1, 42-18.

[5] Avellan, F. , Henry, P. and Ryhming, I.L. , 1987, "A New High-Speed Cavitation Tunnel for Cavitation Studies in Hydraulic Machinery", *Proceedings of International Symposium on Cavitation Research Facilities and Techniques, ASME Winter Annual Meeting,* Boston (USA), FED: Vol. 57, December, 1987, pp 49-60.

[6] Karimi A. and Avellan F., 1986, "Comparison of Erosion Mechanisms in Different Types of Cavitation", *Wear*, Vol. 113, No. 3, pp 305-322.

[7] Avellan F. and Karimi A., 1987, "Dynamics of Vortex Cavitation involved in the Erosion of Hydraulic Machines" *Proceedings of 7th Int. Conf. on Erosion by Liquid and Solid Impact,* 6-10 September 1987, Cambridge (UK),.pp 25-1, 25-8.